ELSEVIER

Diamond and Related Materials 11 (2002) 536–544

DIAMOND AND RELATED MATERIALS

www.elsevier.com/locate/diamond

CVD diamond deposition on steel using arc-plated chromium nitride interlayers

J.G. Buijnsters[a,*], P. Shankar[a], W. Fleischer[b], W.J.P. van Enckevort[c], J.J. Schermer[d], J.J. ter Meulen[a]

[a]*Department of Applied Physics, Research Institute for Materials, University of Nijmegen, Toernooiveld 1, 6525 ED Nijmegen, The Netherlands*
[b]*Hauzer Techno Coating BV, Van Heemskerckweg 22, 5928 LL Venlo, The Netherlands*
[c]*Department of Solid State Chemistry, Research Institute for Materials, University of Nijmegen, Toernooiveld 1, 6525 ED Nijmegen, The Netherlands*
[d]*Department of Experimental Solid State Physics III, Research Institute for Materials, University of Nijmegen, Toernooiveld 1, 6525 ED Nijmegen, The Netherlands*

Abstract

This paper reports on hot filament CVD diamond deposition onto steel using arc-plated chromium nitride (CrN) as the interlayer. Direct deposition of diamond onto steel leads to the formation of a non-adhering layer of graphitic soot covered by poor-quality diamond. However, if arc-plated CrN coatings with a thickness of 2.5 μm are used, diamond formation takes place. Adherent and good-quality diamond coatings are obtained after several hours of deposition at a substrate temperature as low as 650 °C. Micro-Raman spectroscopy, scanning electron microscopy, X-ray diffraction and EDAX analysis have been employed to study the phases, morphology, composition, quality and residual stresses of the grown diamond layers and the modified substrate interlayers. The Scotch tape test is used to assess the adhesion of the diamond coatings.

Keywords: Diamond growth and characterization; Steel; Interlayer; Chromium nitride

1. Introduction

As diamond is the hardest and most wear resistant material known today, diamond coatings are very attractive for applications in the cutting and drilling industry. Therefore, many attempts have been made to grow diamond films directly onto relatively cheap steel substrates. So far, these attempts have only resulted in poor quality layers [1–4]. Direct deposition of diamond onto steel is hampered by the following difficulties: (a) the catalytic effect of iron in the preferential nucleation of graphite; (b) the high solubility of atomic carbon in steel at the usually applied deposition temperatures; and (c) the large thermal stresses generated during cooling down after deposition. These stresses are due to the large mismatch in the thermal expansion coefficients of diamond and steel.

A solution to these problems is the use of an interlayer system between the steel substrate and the diamond coating. Ideally, this layer structure should (1) avoid diffusion of Fe towards the surface, (2) allow for diamond nucleation and growth on top of this surface, (3) supply a good bonding to both the diamond layer and the steel substrate and (4) deal with the thermal stresses generated during cooling.

So far, many studies on single interlayer materials have been reported [4–8]. However, the above-mentioned requirements would suggest an interlayer with a gradient in composition and properties, as may be realized by the use of a multi-layered intermediate system. Nesladek et al. obtained good adhesion by means of a Mo/Ag/Nb multilayer structure, which relieves the stress [9]. Using electroplated metal diamond composite interlayers, well-adhering diamond films on (high-speed) steel substrates were reported [10,11]. Glozman et al. produced well-adhering, good quality diamond coatings on alloy steel, using a nitrided chromium interlayer composed of several layered phases [12]. Recently, Negrea and Vermesan stated the use of reactive magnetron sputtered CrN as a buffer layer for diamond deposition onto A2 tool steel [13].

*Corresponding author. Tel.: +31-24-3653-024; fax: +31-24-3653-311.
E-mail address: buijnste@sci.kun.nl (J.G. Buijnsters).

0925-9635/02/$ - see front matter
PII: S0925-9635(01)00628-8

In our previous work, we reported on the use of nitrided chromium as a suitable substrate for diamond growth by the oxyacetylene flame combustion method [14]. In the present study, the potential of PVD deposited chromium nitride interlayers for diamond coatings onto steel is explored. High-speed and AISI-type 316 stainless steel samples are coated with arc-plated CrN and diamond deposition is performed in a conventional hot-filament-assisted CVD reactor.

2. Experimental

Disc-shaped high-speed and AISI-type 316 stainless steel samples, 18 mm in diameter and approximately 1.3 mm thick, are used as substrates. The high-speed (toolbit, quality no. 1.3207) steel samples contain 1.25 wt.% C, 4.1 wt.% Cr, 3.1 wt.% Mo, 9 wt.% W, 9 wt.% Co, 3.1 wt.% V and balance Fe, whereas the AISI-type 316 stainless steel samples contain 0.03% C, 18.5% Cr, 13% Ni, 2.5% Mo, 1.0% Si, 2.0% Mn and balance Fe. Onto these steel samples, 2.5 μm thick CrN coatings are deposited by PVD-arc technology in an industrial PVD reactor (Hauzer Techno Coating BV) [15]. PVD-arc plating is performed at a deposition temperature of 250 °C for 3 h. A bias voltage of −50 V is applied and a system pressure of 8×10^{-3} mbar is maintained.

Diamond deposition is performed in a conventional hot-filament-assisted CVD reactor as described elsewhere [16]. Direct deposition of diamond onto the high-speed steel substrates is attempted at a substrate temperature of 650 °C using deposition times of 4 and 8 h. To compare the deposition between CrN arc-plated stainless 316 and high-speed steel samples, diamond deposition runs are performed at 650 °C for 2 and 4 h. In all deposition runs, the CH_4:H_2 volume ratio is fixed at 0.5%, keeping the total pressure at 50 mbar and the total flow rate at 300 standard cm^3 min^{-1}. The TaC filament temperature is kept constant at 2100 ± 20 °C as measured with an optical pyrometer.

Prior to diamond deposition, the substrates are ultrasonically abraded for 5 min in a suspension of 0.25 g of diamond powder (particle size 1–2 μm) in 20 ml of 2-propanol, followed by ultrasonic cleaning in 2-propanol.

The presence of diamond and other solid carbon phases is determined by micro-Raman spectroscopy using an Ar ion laser (514.5 nm) with an output power of 5 mW and a focused laser beam diameter of approximately 2 μm (Renishaw System 1000). The Raman spectra are taken in the 1055–1920 cm^{-1} range. X-Ray diffraction and EDAX analysis are employed to study the composition of the as-deposited substrates. X-Ray diffraction is performed in the θ–2θ geometry with a Brüker-AXS D5005 diffractometer equipped with a graphite diffracted beam monochromator using Cu–Kα radiation of 1.5418 Å. Scanning electron microscopy (SEM) is employed to study the morphology of the substrates and diamond coatings. Using a Philips XL30ESEM-W scanning electron microscope, EDAX spectra are taken by spot analysis. The spot size and other beam parameters are chosen, such that the dead time of the detector is 25–30%. As a qualitative adhesion assessment of the diamond films to the CrN coated steel substrates, Scotch tape tests are carried out several times per sample.

3. Results

3.1. Direct deposition onto steel

To allow for comparison between deposition on bare steel and on the CrN coated steel, direct deposition onto the steel samples was carried out at a substrate temperature of 650 °C. Fig. 1 shows the scanning electron micrographs of the layers formed on the high-speed steel samples after (a) 4 and (b) 8 h of deposition. From Fig. 1a, it can be seen that the layer formed after 4 h is very porous and consists of spherical particles, which are approximately 30–150 nm in size. On top and within this porous layer, small diamond nuclei can be observed, which are approximately 0.2–1.2 μm in diameter and hardly show any facetting. After 8 h of deposition, ball-shaped diamond poly-crystallites are observed on top of the graphite soot. These cauliflower diamonds are 1–5 μm in size and form a very porous diamond layer.

The Raman spectra of these layers are displayed in Fig. 2. After 4 h of deposition (Fig. 2a), two bands (ii) centered on 1573 and 1347 cm^{-1} Raman shift can be seen. These bands correspond to the E_{2g} Raman active mode in graphite (G band) and the disordered vibrational modes at graphite crystallite boundaries (D band), respectively [17,18]. The sharp, first-order diamond Raman line (i) is observed near 1328 cm^{-1} and is accompanied by a broad band, which is attributable to amorphous carbon (iii) centred on 1460 cm^{-1}. An additional band can be seen at 1145 cm^{-1} Raman shift, which is assigned to transpolyacetylene segments at grain boundaries and surfaces [19]. For the layer obtained after 8 h of deposition (Fig. 2b), the zero-phonon diamond peak (i) can be observed at 1328 cm^{-1} Raman shift. A broad band consisting of two components can be seen at approximately 1500 cm^{-1}: the band attributable to amorphous carbon (iii) centred on 1480 cm^{-1} and the G band of graphite (ii) at 1580 cm^{-1}. Although less pronounced than in Fig. 2a, both G and D (1350 cm^{-1}) bands of graphite are still detected and the band resulting from transpolyacetylene segments can be seen at 1140 cm^{-1}.

The adhesion of the graphitic layer to both substrates was assessed by means of the Scotch tape test. In the first test, almost the complete layer was immediately

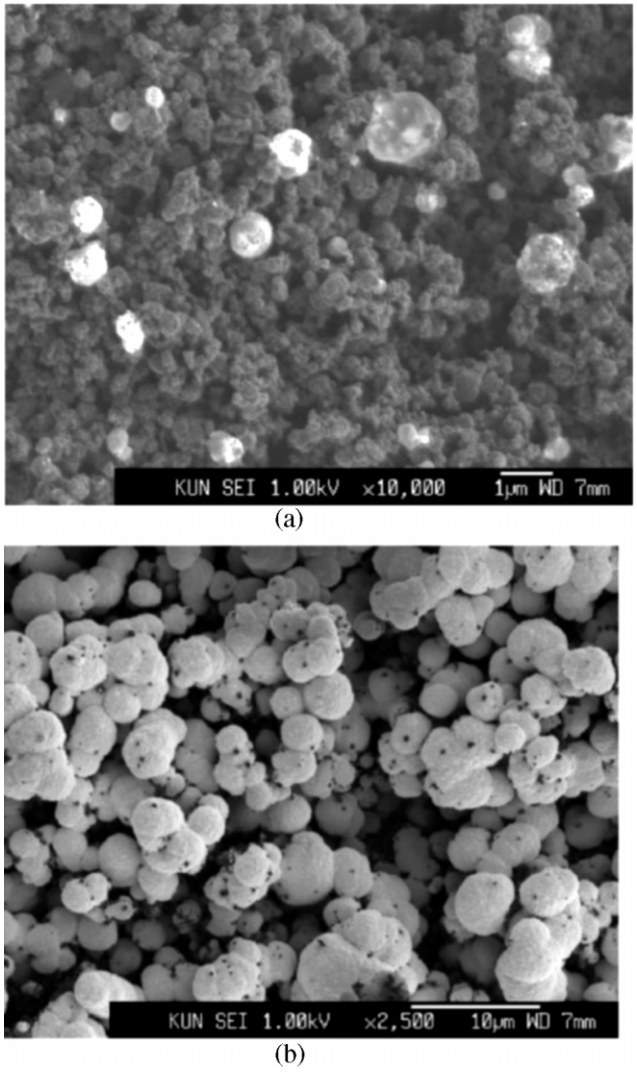

Fig. 1. Scanning electron micrographs of the deposits formed onto the high-speed steel samples after: (a) 4 and (b) 8 h of direct deposition at 650 °C. Note that (a) is at 10.000× magnification and (b) at 2.500× magnification.

removed by the tape. In the subsequent tests, the remaining small parts were removed as well.

3.2. Diamond deposition on arc-plated CrN coatings

After CrN deposition, the different substrate surfaces show a rough structure which is slightly covered by randomly distributed chromium droplets varying in size from approximately 0.1 to 1.5 μm. The rough CrN coating surface also reveals several open areas, which are approximately 10–30 μm in size.

To investigate whether the CrN arc-plated high-speed and stainless 316 steel substrates can facilitate diamond formation, deposition was carried out, keeping the substrate temperature at 650 °C. After deposition runs of 2 h, well-faceted, micron-sized diamond crystallites are observed on both types of substrates. An almost closed layer is formed on the high-speed steel sample, whereas the layer formed on the AISI-type 316 stainless steel consists of individual, slightly coalescing diamond crystallites.

After 4 h of deposition, jumping off of individual or small groups of initially formed diamond crystallites was observed for the AISI-type 316 stainless steel sample during cooling down. As a result, only individual diamond crystallites can be seen over the entire arc-plated AISI-type 316 stainless steel substrate surface (Fig. 3a). The twinned, individual diamond crystallites vary in size from approximately 0.8 to 3.0 μm and have clear cubo-octahedral facets. At some places, the crystallites start to coalesce and form continuous areas of diamond coating. The average particle density is of the order of 10^6 cm^{-2}. Furthermore, cracks can be seen

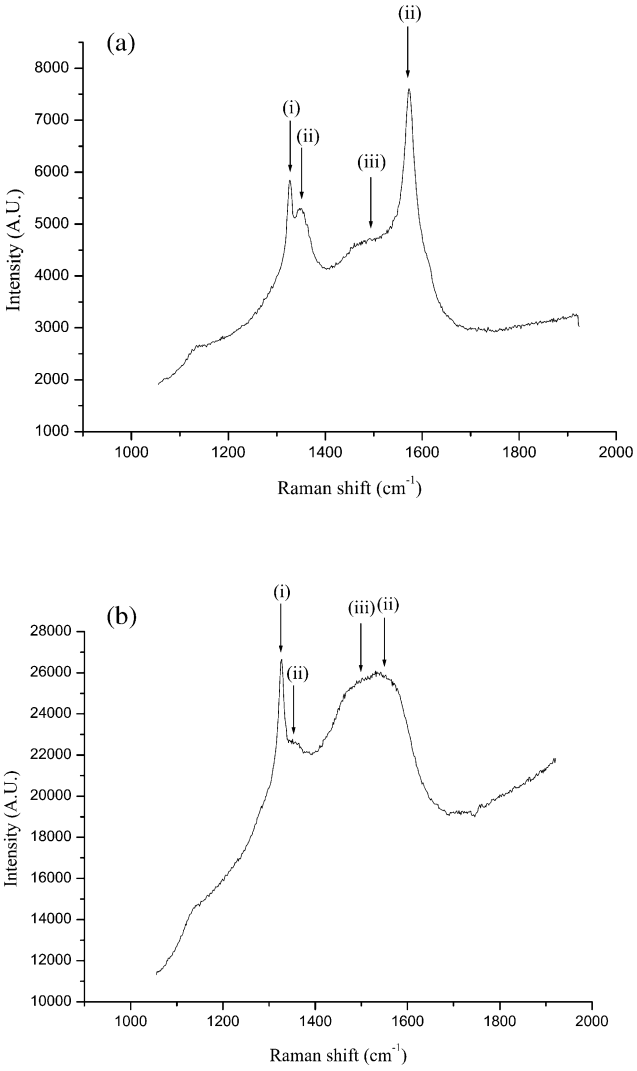

Fig. 2. Raman spectra of the deposits formed onto the high-speed steel samples after: (a) 4 and (b) 8 h of direct deposition (with peak allocation: (i) diamond; (ii) graphite; and (iii) amorphous carbon).

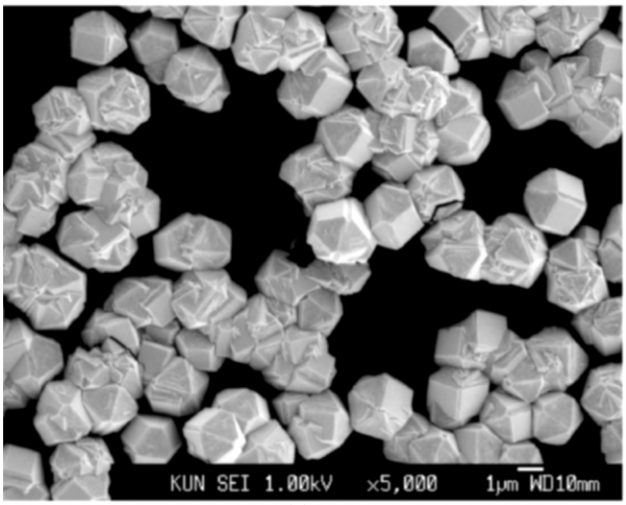

Fig. 3. Scanning electron micrographs of the diamond films on the arc-plated (2.5 μm CrN) (a) stainless 316 and (b) high-speed steel after 4 h of deposition at 650 °C.

within the individual diamond crystallites, which are also heavily twinned on the {111} facets, indicating high stresses.

On the other hand, an almost completely substrate covering diamond coating is formed on the high-speed steel after a deposition time of 4 h (Fig. 3b). The coating consists of randomly oriented, highly-twinned crystallites exhibiting {100} and {111} facets, which have a size varying from approximately 0.2 to 4 μm. The coating is approximately 2.5 μm thick, indicating an overall growth rate of approximately 0.6 μm h^{-1}. In very few areas, tiny parts of the coating (10–30 μm in size) had delaminated, suggesting that the thermal stresses, generated during cooling down, locally exceeded the adhesion strength. The majority of these delaminated parts coincide with the open areas of the arc-plated CrN coating, which are mentioned above.

A representative Raman spectrum of the nuclei present in the adhering parts of the diamond coating after the partial delamination on the AISI-type 316 stainless steel sample, is shown in Fig. 4a. The diamond peak is shifted towards higher wavenumbers and splits into the singlet and doublet signal. The singlet peak (FWHM ≈ 15 cm^{-1}) is found at approximately 1342 cm^{-1} and the doublet (FWHM ≈ 18 cm^{-1}) at approximately 1369 cm^{-1}. A broad band centred on 1560 cm^{-1} due to the presence of amorphous carbon is also detected.

As mentioned above, the deposition run on the arc-plated high-speed steel samples at 650 °C resulted in adherent diamond coatings. A representative Raman spectrum of the nuclei present in the diamond coating deposited on the high-speed steel sample is shown in Fig. 4b. The zero-phonon diamond peak (FWHM ≈ 16 cm^{-1}) is centred at 1345.4 cm^{-1} and shows a shoulder on the left-hand side, which indicates a beginning of splitting up. Due to the presence of amorphous carbon

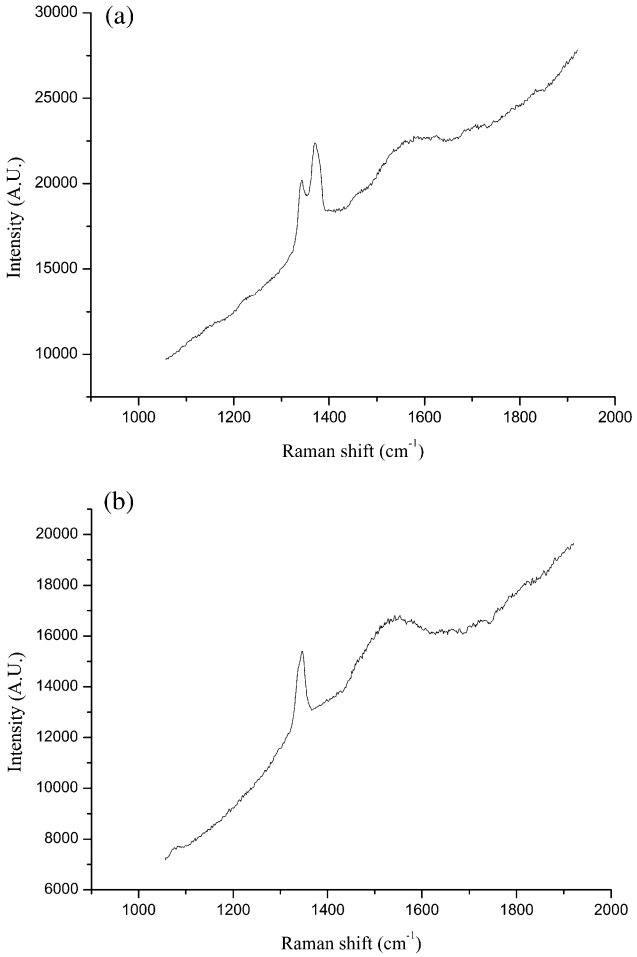

Fig. 4. Representative Raman spectra of the diamond crystallites present in the diamond coatings on the arc-plated steel samples after 4 h of deposition at 650 °C: (a) stainless 316 steel; and (b) high-speed steel.

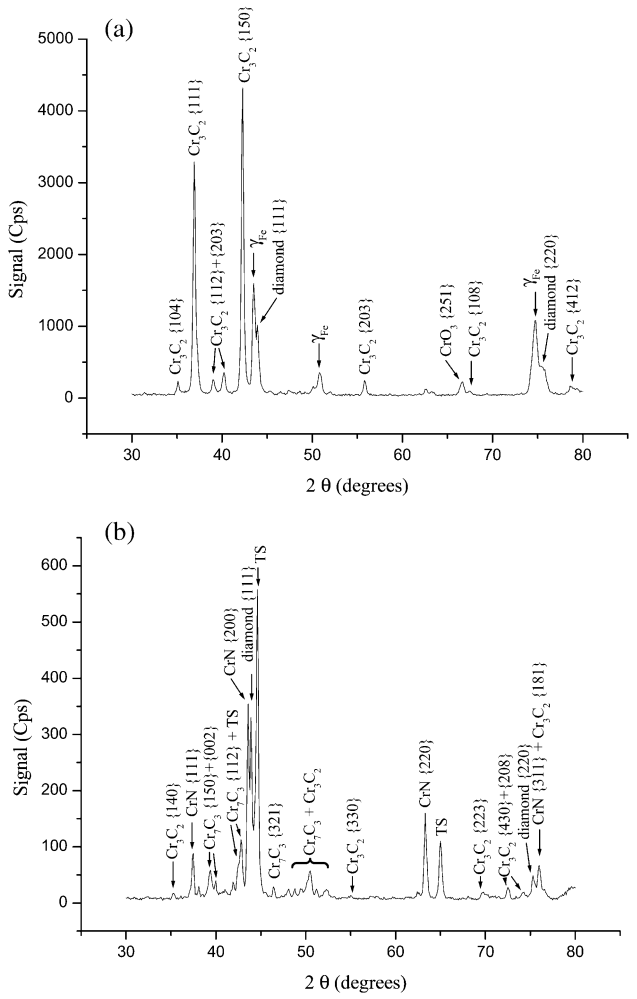

Fig. 5. XRD pattern of the diamond film and interlayer system on: (a) the AISI-type 316 stainless steel; and (b) high-speed tool steel after 4 h of deposition at 650 °C.

within the diamond film, a broad band centred at approximately 1550 cm^{-1} can also be observed.

Fig. 5 displays the X-ray diffraction patterns of the diamond film and interlayer system on both types of steel substrates after 4 h of deposition at 650 °C recorded using Cu–Kα X-rays (1.5418 Å). In Fig. 5a, the diamond {111} and {220} peaks at $2\theta = 43.9°$ and $2\theta = 75.3°$, respectively, are clearly visible for the AISI-type 316 stainless steel substrate. The peaks attributable to the austenitic iron at $2\theta = 43.5$, 50.8 and 74.8° are indicated by γ_{Fe}. The presence of Cr_3C_2 as the dominant carbide phase, formed by interlayer modification during the diamond deposition process, is very clear. Next to the Cr_3C_2 phase, CrO_3 is also detected, although its low intensity points towards a low volume fraction. No diffraction peaks related to CrN are found. For the high-speed steel (see Fig. 5b), the diamond {111} and {220} peaks at $2\theta = 43.9°$ and $2\theta = 75.3°$ are observed. The peaks at $2\theta = 42.8$, 44.6 and 65.0°, attributable to the tool steel, are indicated by TS. Peaks related to the interlayer CrN are detected at $2\theta = 37.5$, 43.6, 63.3 and 76.0°. For the high-speed steel, both Cr_3C_2 and Cr_7C_3 carbide phases are seen.

For both types of steel substrates EDAX analysis shows that carburisation of the CrN interlayer takes place. The nitrogen in CrN at the exposed surface is almost completely substituted with carbon. For the chromium rich surface (AISI-type 316 stainless steel), the nitrogen in CrN is also substituted with small amounts of oxygen. This can be derived from Fig. 6a, which shows the EDAX spectrum of an uncoated spot at which the diamond film delaminated from the stainless steel substrate during cooling down. Approximately 38 at.% carbon and 12 at.% oxygen are calculated from the EDAX spectrum using the Phil-Row-Z model for quantitative analysis.

EDAX analysis of the deposited diamond films/crystallites on both the AISI-type 316 stainless steel and the high-speed steel shows only the presence of C. From Fig. 6b, which shows the EDAX spectrum of the diamond film on the high-speed steel, it is clear that no additional peaks apart from C could be seen up to 5.80 eV. This confirms the absence of elements like O, N, or Ta (filament contamination) in the deposited diamond film.

The Scotch tape test is used to evaluate the adhesion strength of the diamond coatings to the substrate. The

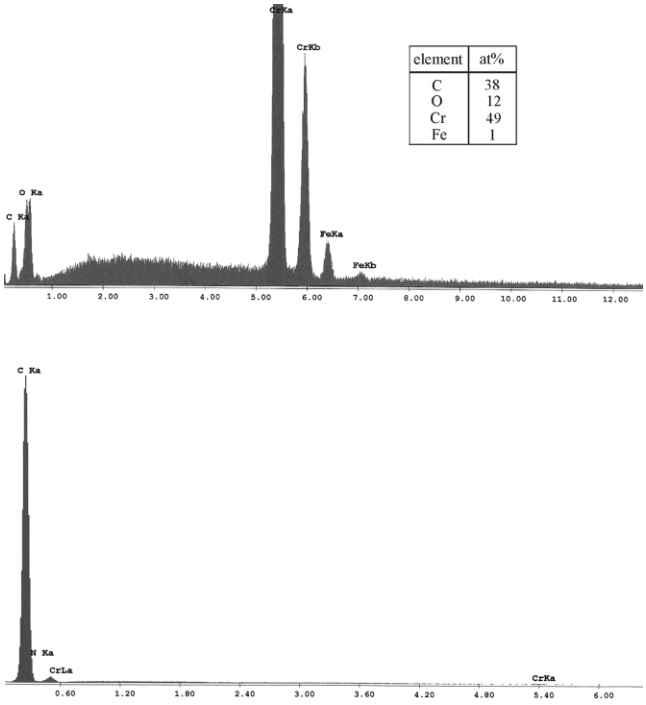

Fig. 6. EDAX spectrum of: (a) an uncoated area on the AISI-type 316 stainless steel; and (b) the diamond film deposited on the high-speed tool steel after 4 h at 650 °C (energy unit is keV).

coatings, as shown in Fig. 3a,b, completely survive all five subsequent tests: no removal at all.

4. Discussion

4.1. Direct deposition onto steel

Direct deposition of diamond onto the steel samples leads to the formation of graphitic soot in the beginning of the deposition process. This is due to the catalytic effect of Fe in the preferential nucleation of graphite. In similar deposition studies on uncoated steel [1,20], it was stated that diamond films can nucleate and grow on top of a layer of graphitic soot, as soon as this layer reaches a critical thickness. In our deposition studies, we observe that after 4 h of deposition at 650 °C, small diamond crystallites ($\sim$0.2–1.2 μm) are formed on top of the graphite soot. After 8 h of deposition, a porous layer consisting of cauliflower shaped diamond poly-crystallites is formed on top of the graphite soot. From the Raman spectra shown in Fig. 2, the diamond peak centres (1328 cm^{-1}) indicate a residual tensile stress. We suggest that the net tensile stress does not originate from the difference in thermal expansion coefficients of graphite and diamond, as only individual cauliflower shaped diamond particles are formed. Besides, the overall expansion of graphite is supposed to be larger than that of diamond and would therefore result in compressive stress, leading to a shift in opposite direction. The peak shift is most likely caused by intrinsic defects in the diamond crystallites, which induce tensile stresses. Phonon confinement may also contribute to the shift towards lower frequencies. If the domain size of the diamond crystallites is in the order of 5 nm, a substantial peak shift and broadening is predicted [21]. From the SEM micrograph of Fig. 1b, it can be observed that the domain sizes of the poly-crystallites are less than approximately 150–200 nm in size. However, as the exact domain size of the crystallites in the poly-crystalline diamond particles can not be detected, we cannot conclude whether phonon confinement is the main reason for the observed shift to lower wavenumbers. Intrinsic tensile stress resulting from grain boundary interactions is to be expected, but these interactions will probably only contribute for a small fraction to the overall residual tensile stress acting on the cauliflower shaped diamond nuclei.

Even though the growth conditions were such that a closed diamond film has grown on top of the graphite layer, the adhesion of the deposit is found to be nil. In our view it is therefore best to avoid the formation of graphite by the use of an interlayer structure.

Our investigation is focused on establishing the applicability of arc-plated CrN coatings with a thickness of 2.5 μm as a diamond hosting layer on steel substrates. We find that it is indeed possible to grow good-quality diamond films on this multilayer system.

4.2. Stresses in the diamond layers grown on CrN coated substrates

From the Raman spectra of the deposited films as depicted in Fig. 4, it can be concluded that the CrN barrier layer has favoured the formation of diamond. For the stainless 316 steel samples, the diamond peak was found to split and to shift to higher wavenumbers. This effect is caused by the residual compressive stress acting on the diamond films after cooling down. Ager and Drory reported a model, which describes the splitting of the triply degenerated Raman diamond peak under biaxial stress [22]. The following equations for biaxial stress (τ) in a polycrystalline diamond film were put forward:

$$\tau = -1.08\ \text{GPa/cm}^{-1}(\upsilon_s - \upsilon_0) \quad \text{for the singlet phonon} \tag{1a}$$

$$\tau = -0.384\ \text{GPa/cm}^{-1}(\upsilon_d - \upsilon_0) \quad \text{for the doublet phonon} \tag{1b}$$

with $\upsilon_0 = 1332\ cm^{-1}$ and υ_s and υ_d the position of the singlet and doublet peaks, respectively.

For the diamond layer on the CrN coated AISI-type 316 stainless steel samples, these equations yield biaxial stress values of 11 and 14 GPa as derived from the maxima of the singlet (1342 cm^{-1}) and doublet (1369 cm^{-1}) peaks, respectively. The Raman spectrum of the nuclei in the film deposited on the arc-plated high-speed steel samples (Fig. 4b) exhibits a single diamond peak at 1345.4 cm^{-1}. This corresponds to a residual compressive stress, which is in the order of 4 GPa. The lower stress for the diamond coating on the high-speed steel is also consistent with the lack of cracks within the individual crystallites and with the SEM observations of the lesser number of twins in the diamond crystallites in comparison to the diamond film on the arc-plated AISI-type 316 stainless steel.

The residual compressive stresses acting on the deposited films, as derived from the Raman peak positions of both steel samples, is the sum of the thermal stress σ_{th} and internal stress components $\Sigma\sigma_{in}$. As the diamond films were deposited under similar conditions and the morphology and crystallite sizes are nearly the same, we assume that the intrinsic stress components $\Sigma\sigma_{in}$ cannot account for the large difference in residual compressive stresses on the diamond films grown on the high-speed and the stainless 316 steel substrates. Therefore, we suggest that this difference in stress is mainly caused by the thermal component σ_{th}.

The thermal stress σ_{th} component arises from the difference in thermal expansion coefficients of the dia-

mond film, CrN and the steel substrates. The thermal stress of a thin diamond layer on top of a thick substrate, induced by a quench from temperature T_2 to T_1 ($= T_{\text{room}}$) can be approximated by

$$\sigma_{\text{th}} = \frac{E}{1-\upsilon} \int_{T_1}^{T_2} \left(\alpha(T)_{\text{s}} - \alpha(T)_{\text{f}}\right) \mathrm{d}T \qquad (2)$$

where $E = 1050$ GPa and $\upsilon = 0.07$ are Young's modulus and Poisson's ratio of diamond, respectively [23]. $\alpha(T)_{\text{f}}$ and $\alpha(T)_{\text{s}}$ are the thermal expansion coefficients of the CVD diamond film and the chromium nitride substrate, respectively. Since the temperature dependence of $\alpha(T)_{\text{s}}$ is not known, in first approximation we use the room temperature values of the thermal expansion coefficients of CVD diamond and CrN ($\alpha(T)_{\text{f}} = 1.0\times10^{-6}$ K^{-1} and $\alpha(T)_{\text{s}} = 2.3\times10^{-6}$ K^{-1}). This gives a calculated thermal stress of 1.0 GPa, which is much lower than the stresses derived from the Raman spectra. If, instead of the thermal expansion coefficient of CrN, the room temperature value of the expansion coefficient of the AISI-type 316 stainless steel ($\alpha_{\text{s}} \approx 16\times10^{-6}$ K^{-1}) is substituted in Eq. (2), a stress value of 12 GPa is obtained. This corresponds well to the values of 11 and 14 GPa derived from the Raman spectrum displayed in Fig. 4a. The value of α_{s} of the high-speed steel is not known exactly, but is supposed to be approximately $\alpha_{\text{s}} \approx 12\times10^{-6}$ K^{-1}. The difference in thermal expansion coefficients of the steel substrates is therefore probably the main reason for the observed differences in residual compressive stress of the deposited diamond films. From this point of view, the use of Eq. (2), with α_{s} substituted by $\alpha_{\text{interlayer}}$, is very limited and should be handled with the utmost care. As, during cooling down of the stainless 316 steel sample, diamond crystals got detached from the substrate at the interface with the CrN, we can conclude that CrN follows the expansion and contraction of the steel substrate. This behaviour was observed also by Negrea and Vermesan [13]. Therefore, we think that the use of Eq. (2) with $\alpha_{\text{s}} = \alpha_{\text{steel}}$ is verified.

From Eq. (2), the thermal stress on CrN due to the differential expansion with the AISI-type 316 stainless steel results in only approximately 3.4 GPa. Although the thermal expansion coefficient of diamond and CrN are nearly similar, the large differences in the thermal stress arise from the difference in their elastic modulus. The Young's modulus of diamond is approximately 1050 GPa, while that for CrN is only approximately 270–290 GPa. The high elastic modulus of diamond in combination with the large difference in thermal expansion results in the large residual stresses. Further, it is also known that the residual stress on thin films is maximal at the interface and decreases towards the surface [24]. Hence, the maximum residual thermal stress is expected at the diamond/CrN interface. It is to be realized that the residual stress of 11 GPa on the diamond film, estimated from the Raman shift, is only an averaged value over the entire film thickness. The actual residual stress at the diamond/CrN interface is expected to be even higher and therefore results in delamination. This explains clearly the observed delamination at the diamond/CrN interface rather than at the CrN/steel interface.

4.3. Composition and structure of interlayer

X-Ray diffraction and EDAX analysis show that, due to in-diffusion of carbon, the nitrogen in the exposed CrN interlayer surface is almost completely substituted by carbon (and small amounts of oxygen are found in the case of the 316 stainless steel). This is more significant for the AISI-type 316 stainless steel than for the high-speed steel. EDAX analysis on regions of the 316 stainless steel substrate where diamond was delaminated shows predominantly only Cr, C and O. No peaks from Fe and other steel components are seen. This suggests that the exposed surface on the delaminated parts is not steel, but is only the carburized phase of CrN. This therefore indicates that the CrN interlayer is still intact, even on regions of the AISI-type 316 stainless steel where the diamond film partially delaminated. The delamination occurs at the diamond/CrN interface and not at the CrN/316 stainless steel interface. So, the adhesion between the diamond film and the CrN interface is the limiting factor for diamond deposition in our CrN/steel system.

X-Ray diffraction of the high-speed steel shows that the X-ray intensity from the Cr_3C_2 phase is much smaller than that from the Cr_7C_3 phase. This indicates that Cr_7C_3 (30 at.% carbon) is the predominant carbide at the interlayer on arc-plated tool steel, in contrast to Cr_3C_2 (40 at.%) on arc-plated 316 stainless steel. The carbon atom percent in Cr_3C_2 is 40% and is close to the observations made by EDAX analysis (38 at.%) of the AISI-type 316 stainless steel. The formation of Cr_3C_2 and Cr_7C_3 phases during diamond deposition on a similar layer system was also revealed by Fayer et al. [25]. They used carbon chrome alloy steel with an interlayer system of nitrided chromium as substrate material, which resulted in the carburisation of the CrN and Cr_2N nitride layers.

Also, there are no peaks from the CrN phase observed on the diamond coated arc-plated 316 stainless steel, indicating the very thick layer of carbide phases formed over it. This is in contrast to the diamond coated specimen of arc-plated tool steel, where a predominant CrN phase is still observed. From these X-ray diffraction results, we can conclude that the formation of an uniform diamond film over arc-plated tool steels could result in the thinner carbide layer phase, since the CrN is exposed

for lesser time to the methane atmosphere during diamond deposition. In contrast, the longer incubation periods for diamond deposition on arc-plated 316 stainless steel can result in the formation of very thick carbide phases with higher carbon stoichiometry (40 at.%) compared to those on tool steel (30 at.%).

Carburisation of the CrN interlayer is determined by the in-diffusion of atomic carbon. The rate of carburisation and thus the local carbon supersaturation of the sample surface influence the early stages of diamond formation. As mentioned above, the incubation time for diamond formation on the high-speed steel is shorter than on the austenitic stainless steel. The difference in exposure time of the CrN interlayer to carbon atmosphere can be the reason for the observed difference in adhesion of the diamond films. The origin of the shorter incubation time for the high-speed steel is not known and needs further research.

The thermal expansion coefficients of the chromium carbides are high in comparison to the ones of diamond and CrN. From literature, the thermal expansion coefficient of the Cr_3C_2 phase is known: $\alpha_{Cr3C2} = 10.6 \times 10^{-6}$ K^{-1} [26]. The high value of the thermal expansion coefficient can result in high thermal stresses at the diamond/interlayer interface and in delamination of the diamond film. Therefore, the formation of a thick intermediate carbide layer is disadvantageous and should be avoided.

On the overgrown austenitic stainless steel substrates, small amounts of CrO_3 are also detected. This phase is probably present as the passivating oxide layer on the 316 stainless steel itself. In-situ removal of this oxide film prior to CrN deposition is being attempted for future studies.

As very few parts of the diamond coating on the high-speed steel sample delaminated during/after cooling, at some very limited areas the residual stresses still exceeded the bonding strength. As pointed out before, some seemingly delaminated areas are most likely a result of the local absence of CrN. The delamination process and its origins are currently studied in detail.

5. Conclusions

In this study, the use of PVD coated CrN interlayers for hot filament CVD diamond deposition on steel substrates was investigated. Direct deposition of diamond onto steel was shown to result in the formation of non-adhering graphitic soot. When arc-plated CrN coatings with a thickness of 2.5 μm were used, adhering, good-quality diamond coatings could be grown. By means of micro-Raman spectroscopy, residual compressive stresses were observed within the diamond coatings, presumably resulting from the mismatch in thermal expansion coefficients of the diamond coating and the steel substrates. X-Ray diffraction and EDAX analysis showed the presence of mainly Cr_3C_2 on the AISI-type 316 stainless steel, whereas Cr_7C_3 is the dominant carbide phase on the high-speed tool steel. The use of interlayer CrN is suitable for the ferritic high-speed steel but does not result in a continuous diamond film for the austenitic AISI-type 316 stainless steel.

Acknowledgments

The authors wish to thank Leander Gerritsen for his technical support. This work was performed as part of the research program of the Netherlands Technology Foundation (STW) with financial support from the Netherlands Organization for Scientific Research (NWO).

References

[1] P.S. Weiser, S. Prawer, A. Hoffman, R.R. Manory, P.J.K. Paterson, S.A. Stuart, J. Appl. Phys. 72 (1992) 4643.
[2] T.P. Ong, R.P.H. Chang, Appl. Phys. Lett. 58 (1991) 358.
[3] H.C. Shih, C.P. Sung, C.K. Lee, W.L. Fan, J.G. Chen, Diamond Relat. Mater. 1 (1992) 605.
[4] Q.H. Fan, A. Fernandes, E. Pereira, J. Gracio, Diamond Relat. Mater. 8 (1999) 1549.
[5] Q.H. Fan, A. Fernandes, J. Gracio, Diamond Relat. Mater. 7 (1998) 603.
[6] J. Spinnewyn, M. Nesladek, C. Asinari, Diamond Relat. Mater. 2 (1993) 361.
[7] J. Ahn, F.H. Tan, H.S. Tan, Diamond Relat. Mater. 2 (1993) 353.
[8] H. Chen, M.L. Nielsen, C.J. Gold, R.O. Dillon, J. DiGregorio, T. Furtak, Thin Solid Films 212 (1992) 169.
[9] M. Nesladek, C. Asinari, J. Spinnewyn, R. Lebout, R. Lorent, M. D'Olieslaeger, Diamond Relat. Mater. 3 (1994) 912.
[10] L. Schäfer, M. Fryda, T. Stolley, L. Xiang, C.-P. Klages, Surf. Coat. Technol. 116-119 (1999) 447.
[11] C.R. Lin, C.T. Kuo, Diamond Relat. Mater. 7 (1998) 903.
[12] O. Glozman, A. Berner, D. Schechtman, A. Hoffman, Diamond Relat. Mater. 7 (1998) 597.
[13] G. Negrea, G. Vermesan, J. Optoelectr. Adv. M. 2 (2000) 698.
[14] J.G. Buijnsters, F.M. van Bouwelen, J.J. Schermer, W.J.P. van Enckevort, J.J. ter Meulen, Diamond Relat. Mater. 9 (2000) 341.
[15] T. Hurkmans, D.B. Lewis, J.S. Brooks, W.D. Munz, Surf. Coat. Technol. 87-8 (1996) 192.
[16] W.J.P. van Enckevort, G. Janssen, L.J. Giling, J. Cryst. Growth 113 (1991) 295.
[17] M.S. Dresselhaus, G. Dresselhaus, K. Sugihara, I.L. Spain, H.A. Goldberg, in: M. Cardona (Ed.), Graphite Fibers and Filaments, Springer–Verlag, Berlin, 1988.
[18] M. Endo, T. Koyama, Y. Hishiyama, Jpn. J. Appl. Phys. 15 (1976) 2073.
[19] A.C. Ferrari, J. Robertson, Phys. Rev. B 63 (2001) 121405.
[20] P.S. Weiser, S. Prawer, Diamond Relat. Mater. 4 (1995) 710.
[21] J.W. Ager, M.D. Drory, Phys. Rev. B 48 (1993) 2601.

[22] J.W. Ager, D.K. Veirs, G.M. Rosenblatt, Phys. Rev. B 43 (1991) 6491.
[23] P.H. Tan, Y.M. Deng, Q. Zhao, W.C. Cheng, Appl. Phys. Lett. 74 (1999) 1818.
[24] Q.H. Fan, J. Gracio, E. Pereira, Diamond Relat. Mater. 9 (2000) 1739.
[25] A. Fayer, O. Glozman, A. Hoffman, Appl. Phys. Lett. 67 (1995) 2299.
[26] I.K. Kikoin (Ed.), Tablitzi fisicheskih velichin, Atomizdat, Moskow, 1976.